ANL-TRANS-947

Conf-730823--20

ARGONNE NATIONAL LABORATORY

Argonne, Illinois

FISSION OF MEDIUM AND HEAVY NUCLEI INDUCED BY HEAVY IONS, Ar and Kr

(FISSION DE NOYAUX DE MASSE MOYENNE ET LOURDE INDUITE PAR IONS LOURDS Ar ET Kr)

By

F. Hanappe, C. Ngo, J. Peter and B. Tamain

Source: IAEA/SM-174/41, International Atomic Energy Agency, Third Symposium on Fission Physics and Chemistry, Rochester, New York, 13-17 August 1973

NOTICE

This report was prepared as an account of work sponsored by the United States Government. Neither the United States nor the United States Atomic Energy Commission, nor any of their employees, nor any of their contractors, subcontractors, or their employees, makes any warranty, express or implied, or assumes any legal liability or responsibility for the accuracy, completeness or usefulness of any information, apparatus, product or process disclosed, or represents that its use would not infringe privately owned rights.

Translated from French

by

STS Incorporated

November 1973

MASTER

DISTRIBUTION OF THIS DOCUMENT IS UNLIMITED

STS INCORPORATED
SCIENTIFIC TRANSLATION SERVICE
formerly Technical Library Research Service
Ann Arbor, Michigan

FISSION OF MEDIUM AND HEAVY NUCLEI INDUCED BY HEAVY IONS, Ar AND Kr

By F. Hanappe, C. Ngo, J. Peter and B. Tamain

Institut de Physique Nucleaire. B.P. No. 1, 91406-Orsay, France

Translated from the French
For Argonne National Laboratory
P. O. No. 773790
Letter Release No. 1

STS Order No. 14405

STS
Ann Arbor, Michigan

STS INCORPORATED
SCIENTIFIC TRANSLATION SERVICE
formerly Technical Library Research Service

IAEA/SM-174/42

FISSION OF MEDIUM AND HEAVY NUCLEI INDUCED BY HEAVY IONS, Ar AND Kr

By F. Hanappe*, C. Ngo, J. Peter and B. Tamain**
Institute of Nuclear Physics
B.P. No. 1,91406 - Orsay, France

International Atomic Energy Agency
Third Symposium on Fission Physics and Chemistry
Rochester, New York, 13-17 August 1973

I. Introduction

The use of heavy ions to induce fission at average excitation energy is of interest for several reasons.

The first is to permit a study of the fission of very heavy nuclei ($Z > 100$), formed either by complete fusion between a heavy target and the projectile,+ or by partial fusion (transfer of a large part of the projectile to the target). This would obviously permit broadening of the range of nuclei for which we presently have experimental fission data (Z from ~ 75 to 100), and to verify whether the theories concerning fission developed from the data of this interval are applicable to heavier nuclei. Complete fusion of ^{40}Ar and ^{238}U might lead to ^{278}X, and $^{84}Kr + ^{238}U$ would yield ^{322}X. Inversely, the observation of deexcitation by fission of these nuclei is the simplest means to demonstrate that they have actually been produced.

Secondly it is of interest in supplying very significant angular momenta. Present fission theories do not predict the effect of angular momentum on the mass and energy distributions of the fragments, and the experimental data can establish what this effect may be.

We therefore began two series of experiments: the first was conducted with argon ions, the second with krypton ions. In both cases, we obtained the fission cross-sections of the compound nucleus on a series of target nculei. For the argon-initiated reactions, we

+) In the absence of a detailed description of the experimental setup, the word "projectile" has been retained in this translation.--Tr.

were able to make measurements at several bombarding energies, and the effect of the angular momentum on the fission barrier height was studied. In the case of krypton, it is very difficult to form a fusion nucleus with a heavy target, and a new type of reaction was observed: partial fusion between the projectile and the target, and then disintegration into two fragments of masses similar to those of the projectile and the target. The effect of the mass of the target nucleus on this phenomenon was studied.

Finally, in the case of argon-initiated reactions, we have determined the mass and kinetic energy spectra of fragments produced by fission of the compound nucleus. The values of the mean total kinetic energies, and the total kinetic energy and mass distribution widths were compared with the predictions of different models.

II. Experiments

The experimental method used was the same for all measurements discussed here. We will give only a summary description of it; details may be found elsewhere [1,2].

A. Experimental Device

Three surface barrier detectors, X, Y1 and Y2, were placed at angles θx, $\theta y1$, and $\theta y2$ with respect to the beam direction. They form coincidence detectors (XY1 or XY2) for the fission fragments or other reaction products (elastic scattering, transfer) originating from a same event in the target. The linear pulse heights corresponding to Ex, Ey1 or Ey2, as well as the difference in flight time between the two fragments ($\Delta TV1$ or $\Delta TV2$) were recorded on magnetic tape. This difference in flight time was used to determine the contribution of random events [1]. The detector background was reduced to a minimum: each was shielded by a magnetic field and a nickel sheet of 80 $\mu g/cm^2$ which eliminate electrons and soft x-rays, respectively, due to entry of the beam in the target.

Detector X was held at a fixed angle, and its angle of aperture $\Delta\theta x$ in the reaction plane was small. Detectors Y covered an angular interval $\Delta\theta y$ of 10° each, and were placed at 20° from one another so as to permit scanning of a broad angular correlation interval in few measurements. In a few cases, $\Delta\theta y$ was reduced to 3°. The angular correlations were estimated in advance by applying the initial momentum to the fusion nucleus and by assigning the kinetic energy predicted by the liquid drop theory [3] to the fragments.

This correlation depends on the mass ratio. We scanned an angular interval very generously enclosing the predicted interval.

The effect of neutron evaporation from the fragments is to remove the fragments produced by the same event from the reaction plane. In order to collect them, the angle of aperture of detector X in the direction perpendicular to the reaction plane ($\Delta\Phi x$, Fig. 1) was equal to $\pm$ 7.5° and that of detectors Y was only 2°. Calculation of the possible angular deviations between the fragments evaporating the greatest number of neutrons indicates that this aperture $\Delta\Phi x$ is sufficient so that no fragments will be lost; this was confirmed by measurements of correlation with the aid of a localizing detector in the direction perpendicular to the reaction plane.

B. Data Processing

The hypothesis is made that the detected event has only two end products, of which the sum of masses is equal to that of the sum of masses of the input channel (projectile + target). Deexcitation by evaporation of neutrons or light charged particles of these two reaction products may slightly modify their mass, energy, and direction, but no third product of significant mass is produced during the reaction. The system formed by the group of nucleons of the projectile and target-nucleus which gives rise to the two end products (by whatever process) thus has the momentum of the projectile. Consequently, in the laboratory system, the two end products should form an angle θxy very different from 180° (each product being forward-scattered). Depending on the cases, θxy will vary from 140 to 60°. The angles observed between the reaction products indeed have values close to these estimates. In contrast, the deviation in the direction perpendicular to the reaction plane (Φ) is small; if a third particle of significant momentum was produced, the two detected products would only exceptionally be coplanar with the initial direction of the projectile. It can thus be concluded that the hypothesis made is correct.

From this hypothesis and the measured energies and angles, we can calculate the masses of the two products and their energies and angles of emission in the center of mass system. We will not review the kinematic relations used [2].

A first problem of the method resides in the response of the surface barrier detectors to heavy and high-energy ions. In fact,

it is known that this response depends on the mass of the detected nuclei. Since the masses are not known initially, it is necessary to perform a series of iterations in order to obtain a correct determination of both the masses and kinetic energies from the two measured pulse heights. This does not represent a source of errors. In contrast, the fact that the energies of the detected products are high (particularly because of the considerable momentum of the population) can lead to a systematic error. In fact, the calibration methods presently known (Schmitt and Kiker [4], Steinberg et al. [5]) are based on the response of the detectors with ions of lower energies than those which are to be measured. The elastically scattered nuclei (target or projectile or both, depending on the case), of known mass and energy, provide an easy test. We thus compared the results obtained for elastic scattering with the two calibration methods. Moreover, we made a detailed study of the ionization error of the detectors used for ions of heavy mass and high energy [6].

In processing of the data, we took care to take into account the energy losses of each detected product in the target, possibly the target support, and the nickel sheet shielding the detector. This was done in each iteration step from the stopping powers of the table of Northcliffe and Schilling [7], the validity of which was tested in a few cases [6].

A knowledge of the angles θy is far from precise since the angles of aperture are about 10°. Here also, correction by successive approximation was necessary in order to determine the real value of θy. This was done by requiring emission of the two products at 180° from each other in the center-of-mass system.

A last point concerns not the characteristics of a detected event, but the respective proportions of the various events. In fact, a product of defined mass M and velocity Vx detected at angle θx corresponds to an angle $\overline{\theta}x$ and to a velocity $\overline{v}x$ in the center-of-mass system. The products detected at θx originate from different θx (according to $\overline{v}x$). If the angular distribution in the center-of-mass system is not isotropic (for example according to $1/\sin \overline{\theta}$ for fission of a compound nucleus having a high angular momentum), certain categories of events are favored in the laboratory system relative to their real contribution in the center-of-mass system. To limit this deformation, the measurements were made at $\overline{\theta}$ close to 90°, an angle

for which the differential cross-section $d\sigma/d\Omega$ practically does not depend on $\overline{\theta}$. On the other hand, the number of fragments obtained in the solid angle $d\Omega$ is a function of the CMS-LS conversion factor in which $\overline{\theta}x$ and $\overline{v}x$ intervene. This factor was therefore calculated for each detected event. In this way, the correct mass and energy spectra were obtained in the center-of-mass system, within the error of the angle and energy resolution.

The results thus obtained neglect the evaporation of neutrons, either before or after fission. We calculated that the probability of neutron evaporation before fission was very small in all cases. In contrast, a great number ν_T of neutrons can be emitted by the fragments. This number was estimated from the excitation energy available for the fragments, and the mean total kinetic energy of fission could be corrected. However, this was not possible for the mass distributions since the variation of ν with the mass of the fragments was not known.

III. Characteristics of Fission Fragments

It is convenient to present the results in graphic form (total kinetic energy in the CMS x mass of one of the two detected products). These graphs are shown in contour curves in Figs. 1, 2 and 8, where the mass is that of the product reaching the fixed detector X. The fission fragments, distributed around the half mass of that of the fusion nucleus more or less clearly form the known triangles with rounded vertices [8,9].

Moreover, sometimes elastic or inelastic scattering or transfer events are observed. These different patterns appear depending on whether the detection angle θx belongs to or is near the angular intervals $(0°, \theta proj)$ and $(\theta target, 90°)$ in which the projectile and the target, respectively, are elastically scattered with a considerable differential cross-section close to that of Rutherford. In these intervals, the impact parameter is such that the minimum distance of approach is greater than or equal to the sum of the effective interaction radii of the projectile and the target. For smaller impact parameters transfer reactions are produced, the products of which are in the vicinity of $\theta proj$ and $\theta target$.

Figs. 2 and 3 show three different cases. The distinction between fission fragments and elastic scattering is easy, but this is not always the case for transfer or inelastic scattering products.

Therefore, for the Ar + Mo system, the masses of the projectile and target are sufficiently similar for the scattering or transfer events to perturb the bound of the fragment mass distribution. For the heavier targets (Pr, Ho), this problem practically no longer arises. For the very heavy systems (Th or U + Ar) at 250 MeV, the kinetic fission energies are close to the scattering target, and the mass distribution width is such that the distributions are perturbed by the transfer events. Finally, it has not been ruled out that some events of the type observed with the Kr + Bi system (Fig. 8) exist also for such systems.

A. Angular Correlations

A few of the observed angular correlations are shown in Fig. 4. The smallest angles correspond to the high mass ratios, since the total kinetic energy then is less than that corresponding to fission into two equal fragments. The latter are the most numerous and form the correlation maxima at a larger angle. We have indicated the correlation predicted from the mean kinetic energy for fission into two equal fragments, calculated according to Nix [3]. The predicted angle is smaller than the observed angle; thus, the predicted kinetic energy is smaller than the real value.

B. Mass and Kinetic Energy Distributions

The results for the mean total kinetic energies for the half-widths of the mass and total kinetic energy distributions are listed in Table I.

1. Mean total kinetic energies. In Fig. 5, our mean total kinetic energy values are compared to a group of data obtained by other authors and to the theoretical predictions of Nix, on one hand [3], and Mosel and Schmitt, on the other hand [10]. The energies are relative to fission into two equal fragments.

The theory of Nix uses the liquid drop model and neglects shell effects. In contrast, Mosel and Schmitt correctly predict that these effects are very significant, and become manifest in a high kinetic energy value when the two fragments obtained are almost magic. Our experimental results are much more similar to those of Nix than to those of Mosel. This does not allow the conclusion that the Mosel and Schmitt model is incorrect; most probably, with the high excitation energies involved in our experiments (Table I), the shell effects become negligible. This result is not surprising if one notes, for

Target	Comp. Nucleus	E_{Argon}	E^*	<ECT'>	<ECT>	ECT_{Nix}	ECT_{Mosel}	θ	Γ_M	$\Gamma_{M(Nix)}$	Γ_E	$\Gamma_{E(Nix)}$
Mo	Nd	200	98	93	96	86		1.66	27	33	20	13
"	"	300	169	93	100	"		2.66	47	41	33	16
Sb	Tm	162	58	114	114	104.4		1.05				
"	"	179	72	111	113	"		1.36	31.5	27	18.5	14
"	"	199	86	111.8	114	"		1.58	34.5	29	22.5	15
"	"	226	106	111.7	116	"		1.87	36	32	26.5	16
"	"	300	164	108.9	116	"		2.4	55	36	36.5	18
Pr	^{181}Ir	226	95	131	135	122.8		1.75	47	27.5		17.5
"	"	300	150	125.7	133	"		2.31	55	31	36	19.5
Ho	^{205}As	226	97	145.5	152	142		1.74	46	24	29	18
"	"	300	160	143.4	154	"		2.35	60	28	38	20.5
Au	^{237}Bk	226	71	175.9	183	176.1	160	1.43	45	19	36	19
"	"	250	89	181	190	"	"	1.63	66	21	39	20
"	"	300	133	178.5	190	"	"	2.04	95	23	45	21.5
Bi	^{249}Md	250	80	183	193	188.6	185	1.49	~100		45	
"	"	250	80	193	203	"	"	"				"
Th	^{272}108	250	83	207	218	212.2	246	1.49	90-110		46	
"	"	250	83	214	224	"	"	"				
U	^{278}110	250	82	204.5	217	219.7	233	1.23				
"	"	300	125	203	218	"	"	1.53	100		65	

Table I--Mean total kinetic energies and mass and kinetic energy distribution widths. <ECT'> is the mean energy before neutron emission. <ECT> is the energy corrected for neutron emission. The energy values calculated by Nix, on one hand, and Mosel and Schmitt, on the other hand, as well as the distribution widths calculated by Nix are listed. All energies are in MeV; the mass distribution widths are in amu, the nuclear temperatures in MeV (see text).

example, that in the case of uranium excited at 40 MeV, fission is already essentially of a symmetrical type; particularly, the total kinetic energy has values and a variation with the mass ratio of the fragments different from those obtained for low energy fission [9,12].

Although the effect predicted by Schmitt and Mosel is very significant, one would anticipate that a fraction of the excitation energy would persist at 80 MeV (Table I).

With regard to the predictions of Nix, we note that the calculated energies are underestimated as is true for the nuclei of $Z < 95$. Moreover, the experimental ard theoretical curves representing the variation of the mean total kinetic energy with x (fissionability parameter) have different slopes, the theoretical curve rising more rapidly than the experimental curve.

2. Mass and kinetic energy distribution widths. Since the shell effects seem to be negligible for the reactions of interest to us, it is of advantage to know to what extent the liquid drop theory accounts for other fission characteristics, such as the widths Γ_M and Γ_E of the mass and kinetic energy distributions. It is known that the theory of Nix [3] has meaning only for fissionability parameters smaller than 0.8. When this condition is verified, the experimental and theoretical values of these widths can be compared in Table I and Fig. 6.

Except in the case of molybdenum, the calculated widths are too small and the more so with a higher excitation energy of the compound nucleus. Moreover, the calculated curve representing the variation of Γ_M with the fissionability parameter at constant nuclear temperature decreases while the experimental curve increases. The difference between equivalent curves for Γ_E is marked although less significant. In all cases, the nuclear temperatures have been calculated by deducing from the excitation energy only the value of the fission barrier plus the minimum spin energy which the nucleus must have for fission (see § IV). It was also assumed that no neutron was evaporated before fission. These temperatures are therefore overestimated; a more correct calculation would be to increase only the theoretical-experimental difference, particularly for the large values of the fissionability parameter.

IV. Argon-Induced Fission Cross-Sections and Excitation Functions

The fission cross-sections in question here concern solely fission after complete momentum transfer, i.e., after fusion of the projectile and the target. Moreover, it was assumed that this fusion nucleus attained the thermodynamic equilibrium state of the compound nucleus before undergoing fission. Thus, the fission cross-sections were calculated by considering that the angular distribution of the fragments is proportional to $1/\sin \overline{\theta}$ because of the considerable angular momentum of the fissioning nucleus [8,9]. $1/\sin \overline{\theta}$ is an upper limit since in the vicinity of 0° (or 180°) the differential cross-section remains finite, but even with smaller angular momenta supplied by the 150 MeV α-particles, the overestimate is less than 5% [10].

Our results for the different target + projectile pairs at different energies are listed in Table II: fissionability parameter x, projectile-target interaction barrier, excitation energy of the compound nucleus, fission barrier, measured fission cross-section, calculated reaction cross-section, and, finally, maximum possible angular momentum of the compound nucleus and maximum angular momentum actually attained (critical). The fissionability parameters are calculated by the relation $x = Z^2/50.13\ A$. The interaction barriers V were calculated with an effective interaction radius r_e of 1.45 mf [12,13]. The excitation energies were obtained from the mass deficits of the table of Myers and Swiatecki [14], which also furnished the values of the fission barriers of the compound nucleus. The reaction cross-sections are calculated by the relation $\sigma_R = \pi(R_1+R_2)^2(1-\frac{V}{E})$ where R_1 and R_2 are the radii of the two nuclei from the input channel, and E is the available kinetic energy in the center-of-mass system.

The errors indicated for the values of the fission cross-sections have several sources: target thicknesses, solid angles but, especially in certain cases, difficulty in distinguishing the fragments originating from very asymmetrical fissions of transfer products (Figs. 1 and 2).

This table can be divided into two parts. For the compound nuclei of mass smaller than 200, fission is not the deexcitation process chosen by all nuclei. In contrast, for the heavier nuclei

almost all of the nuclei resulting from fusion of the projectile and target undergo fission in one stage of the deexcitation chain.

A. Compound Nuclei of Mass Less than 200

In these cases, the fission barrier is high (i.e. much higher than the binding energy of the last neutron), which implies that fission is no longer the dominant deexcitation process. In fact, it is even surprising from the start to observe such large fission cross-sections when the corresponding barriers exceed 20 MeV (see the case of antimony, for example). An angular momentum effect is involved here since it is known that the latter lowers the effective fission barriers:

$$\Delta B_f = E_{RO} - E_{RS}$$

E_{RO} and E_{RS} are the spin and threshold energies of the spherical nuclei.

According to Halpern and Strutinsky [8]:

$$\Delta B_f = \frac{\hbar^2}{2J_o} I \left[1 - \frac{J_o}{J_+}\right] - \frac{\tau_s}{2}$$

where I = angular momentum of the fusing nucleus

J_o and J_+ = moments of inertia of spherical nuclei, and at the threshold in the direction perpendicular to the deformation axis

τ_s = nuclear temperature

The values of J_+/J_o were obtained from the studies of Cohen and Swiatecki [15].

Fig. 7 shows the variation of the experimental fission cross-section, total reaction cross-section, and reaction cross-section corresponding to the partial waves of angular momentum greater than $J_{Bf=Sn}$ with the incident energy for antimony. $J_{Bf=Sn}$ is the value of the angular momentum for which lowering of the barrier is such that the effective fission barrier is equal to the binding-energy of the last neutron. It can be said that angular momenta smaller than $J_{Bf=Sn}$ make no contributions to the fission cross-section and, reciprocally, that any nucleus having acquired an angular momentum greater than $J_{Bf=Sn}$ is assuredly deexcited by fission. This is obviously very schematic, and Fig. 7 therefore shows the reaction cross-sections corresponding to partial waves of angular momenta greater than $J_{Bf=0}$ and $J_{Bf=2\ Sn}$ (dotted curves). If no critical

Target	Compound nucleus	x	Energy L.S. MeV	Energy C.M.S. MeV	Interaction barrier C.M.S. MeV	E^*	B_f MeV	$\sigma_{F_{mb}}$	σ_R	$\frac{\sigma_F}{\sigma_R}$	σ_{max}	σ_{crit}
^{nat}Mo	Nd	0.528	200	140	93.5	98	39	145±30	1400	0.1	96	(82)
"	"	"	300	209.5	"	169	"	163±15	2350	0.07	151	(83)
^{nat}Sb	Tm	0.586	162	122	109	58	28.5	103±1	450	0.02	53	(>53)
"	"	"	179	135	"	72	"	187±20	840	0.22	74	(>74)
			199	150	"	86	"	510±80	1250	0.4	94	(94)
			226	170	"	106	"	535±50	1620	0.32	114	(98)
			300	226	13"	164	"	620±60	2370	0.26	158	(108)
^{165}Ho	^{205}At	0.702	226	182	135	97	13	860±90	1348	0.64	110	102
"	"	"	300	242	"	160	13	1430±140	2300	0.62	166	139
^{209}Bi	^{249}Md	0.820	250	210	158	80	~0	1110±200	1380	0.81	122	110
^{238}U	$^{278}110$	0.870	250	214	171	82	<0	766±150	1230	0.62	117	92
"	"	0.870	300	257	171	125	<0	1220±120	2043	0.60	166	128

Table II--Fission cross-sections of complete fusion nuclei formed with $^{40}_{18}Ar$ projectiles. The errors indicated are estimates.

Target	Compound nucleus	x	Energy L.S. (MeV)	Energy C.M.S. (MeV)	Interaction barrier, C.M.S. (MeV)	Excitation energy	$\sigma_{F_{mb}}$	$\sigma_{R_{mb}}$	$\frac{\sigma_F}{\sigma_R}$	ℓ_{max} ($\hbar$)	$\frac{d\sigma}{d\Omega}$ (mb/sr)
^{165}Ho	^{249}Lw	0.849	450	298	263	62	~200	800	~0.25	139	
"	"	"	493	327	263	91	(230)	1050	(0,22)	170	(20)
^{186}W	$^{270}110$	0.893	502	346	284	105	(150)	990	(0,15)	173	(15)
^{209}Bi	$^{293}119$	0.965	502	358	312	52	$\lesssim$ 40	800	$\lesssim$ 0.05	157	70
^{238}U	$^{322}122$	0.92	502	371	335	50	< 10	610	<0.02	144	

Table III--Binary fission cross-sections σ_F and differential partial fusion cross-sections $d\sigma/d\sigma$ observed with the ^{84}Kr projectiles. The values in parentheses are from preliminary results. The value σ_R is the total reaction cross-section.

angular momentum existed (as in the case of reactions induced by lighter ions), the fission cross-section curve would fall between the two dotted-line curves of Fig. 7 (although with the possibility of exceeding the upper limit). First of all it is observed that the experimental fission cross-section indeed begins in this range. This result confirms the validity of our calculations. In contrast, for higher incident energy values, the fission cross-section is smaller than the expected value. This result is interpreted in terms of the critical angular momentum and is discussed elsewhere [16]. To review, the critical angular momentum is the value of angular momentum above which production of a fusion nucleus would no longer be possible.

To conclude, we will make the following remark. As the mass of the compound nucleus decreases, the critical angular momentum decreases; in contrast, the angular momentum from which the fission probability is no longer negligible increases (at least up to molybdenum) [36]. Thus, a compound nucleus mass exists below which the fission cross-section is very small (at mean excitation energy). This mass can be placed into the vicinity of 110 uma, i.e., a target in the vicinity of copper for argon-induced reactions.

B. Compound Nuclei of Mass Greater than 200

In this case, nearly all of the nuclei resulting from fusion of the projectile and the target undergo fission either immediately or after evaporation of a neutron or a charged particle. This is because the effective fission barrier (taking the angular momentum into account) is less than or close to the separation energy of the last neutron.

Measurement of the fission cross-section after transfer of complete momentum is thus a measure of the compound nucleus production cross-section or, more generally, of the complete fusion nucleus production cross-section between the projectile and the target.

It is noted that for all cases this cross-section is smaller than σ_R. In each case the value of the critical angular momentum ℓ_{cr} is derived from this, beyond which there would no longer be complete fusion. This value increases with the mass of the fusion nucleus and with the excitation energy. A comparison with other results has shown that ℓ_{cr} also increases with the mass of the projectile, at least up to argon [16].

V. Fission and Partial Fusion Induced by Krypton

Fig. 8 which corresponds to the interaction of 500 MeV ^{84}Kr with a target of ^{209}Bi, shows that very few events are attributable to fission of the compound nucleus ^{293}X. In fact, by taking the few events near a mass ratio of 1 and assuming a broad fission fragment mass distribution of 100 amu, the fission obtained after complete fusion between Kr and Bi amounts to only about 40 mg, i.e., less than 5% of σ_R. A similar result concerning the fusion nucleus $^{322}_{128}X$ (obtained from Kr + ^{238}U) indicated a binary fusion cross-section smaller than 10 mb [17] (Table III). The corresponding value of ℓ_{cr} would be very small.

We performed the same measurements with ^{165}Ho and ^{186}W targets, the results of which will be given at the meeting. It is already apparent that the fission cross-sections after complete fusion and the proportion of the reaction cross-section are greater when the mass of the target is smaller. Let us note that in our experiments this also corresponds to higher energies with respect to the interaction barrier. It is thus possible that the decisive factor would be the energy necessary to cross a fusion barrier which may be higher than the interaction barrier.

This result might in fact mean that the fission of the formed super-heavy excited compound nuclei is essentially a ternary process and consequently inaccessible to our measurements. This hypothesis does not appear unjustified if we extrapolate known results for lighter nuclei [17], but three facts contradict this. On one hand, the complete fusion nuclei of even similar Z and A ($^{278}_{110}X$ and $^{270}_{110}X$) were formed by the reactions ^{40}Ar + ^{238}U and ^{84}Kr + ^{186}W, respectively; very different values of the ratio σ_F/σ_R correspond to these two reactions. On the other hand, for the fusion nuclei lighter than ^{278}X and formed by Ar, the proportion of ternary fission is not very large [16]; however, neither the excitation energy nor the angular momenta supplied by the Kr ions are greater than those due to the Ar ions of ref. [17]. Finally, Fig. 8 shows events other than fission or transfer.

The differential cross-section of these events is large. In the case of Kr + Bi, their total cross-section calculated by assuming an isotropic angular distribution in the center-of-mass system would be equal to σ_R. This is obviously exagerated since there are a large number of other reactions (transfer), and this suggests that their angular distribution has a maximum.

By studying the mass and total kinetic energy distribution of these events, we are struck by the fact that their masses are essentially near those of Kr and of the target. On the other hand, their total kinetic energy is on the order of that expected for highly asymmetrical fission. They might result from the formation of a quasi-molecular state between the interaction barrier and the fusion barrier with a short-half-life. The decay of such a state would lead to fragments with a mass close to those of the input channel since no equilibrium configuration is attained.

References

[1] Cabot, C., Ngo, C., Peter, J., and Tamain, B.: Nucl. Instr. Meth., in press.

[2] Tamain, B.: Thesis in preparation, Orsay.

[3] Nix, J.R.: UCRL 17958.

[4] Schmitt, H.W., Kiker, W.E., and Williams, C.W.: Phys. Rev. 137, B 837 (1965).

[5] Wilkins, B.D., Fluss, M.J., Kaufman, S.B., Gross, C.E., and Steinberg, E.P.: Nucl. Instr. Meth. 92, 381 (1971), and Nucl. Instr. Meth. 99, 320 (1972).

[6] Borderie, B.: Thesis of the Third Cycle, Orsay (1973).

[7] Northcliffe, L.C., and Schilling, R.F., Nuc. Data Tables A7, 233 (1970).

[8] Plasil, F., Burnett, D.S., Britt, H.C., and Thompson, S.G., Phys. Rev. 142, 696 (1966).

[9] Galin, J., Lefort, M., Peter, J., Tarrago, X., Cheifetz, E., and Fraenkel, Z., Nucl. Phys. A134, 513 (1969).

[10] Schmitt, H.W., and Mosel, U., Nucl. Phys. A186, 1 (1972).

[11] Britt, H.C., and Whetstone, S.L., 133, B 603 (1964).

[12] Lefort, M., NGO, C., Peter, J., and Tsmain, B., Nucl. Phys. A197, 485 (1972).

[13] Wong, C.Y., Phys. Lett. 42B, 186 (1972).

[14] Myers, W.D., and Swiatecki, W.J., Nucl. Phys. 81, 1 (1966).

[15] Cohen, S., and Swiatecki, W.J., Annals Phys. 22, 406 (1963).

[16] Lefort, M., Le Beyec, Y., and Peter, J., IPNO-RC 73-04.

[17] Brandt, R., Angew. Chemie 10, 890 (1971).

[18] Pere Lygin, V.P., Shadleva, N.H., Tretlakova, S.P., Boos, A.M., Brandt, R., Nucl. Phys. A127, 577 (1969).

[19] Sikkeland, T., Arkiv För Fysik 36, 539 (1966).

[20] Cabot, C., Thesis of the Third Cycle, Orsay (1972).

[21] Galin, J., Lefort, M., Peter, J., Tarrago, X., Cheifetz, E., and Fraenkel, Z., Nucl. Phys. A134, 513 (1969).

[22] Britt, H.C., and Whetstone, S.L., Phys. Rev. 133, B 603 (1964).

[23] Britt, H.C., Wegner, H.E., and Judith C. Gursky, Phys. Rev. 129, 2239 (1963).

[24] Plasil, F., Burnett, D.S., Britt, H.C., and Thompson, S. G.: Phys. Rev. 142, 696 (1966).

[25] Schmitt, H.W., Neiller, J.H., and Walter, F.J.: Phys. Rev. 141, 1145 (1966).

[26] Unik, J.P., Cuninghame, J.G., and Croall, I.F., Proceedings of the Second IAEA Symposium on Physics and Chemistry of Fission 717 (1969).

[27] Burnett, S.C., Ferguson, R.L., Plasil, F., and Schmitt, H. W.: Phys. Rev. C 3, 2034 (1971).

[28] Sikkeland, T.: Phys. Letters 31 B, 451 (1970).

[29] Alkhazov, I.D., Kostochkin, O.I., Kovalenko, S.S., Malkin, L.Z., Petrzhak, K.A., and Shpakov, V.I., Sov. Jour. Nuc. Phys. 11, 281 (1970).

[30] Komar, A.P., Bochagov, B.A., Kotov, A.A., Ranyuk, Yu. N., Semenchuk, G.G., Solyalin, G.E., and Sorokin, P.V., Sov. Jour. Nucl. Phys. 10, 30 (1970).

[31] Balagna, J.P., Ford, G.P., Hoffman, D.C., and Knight, J.D., Phys. Rev. Lett. 26, 145 (1971).

[32] John, W., Hulet, E.K., Lougheed, R.W., and Wesolowski, J.J., Phys. Rev. Lett. 27, 45 (1971).

[33] Neiler, J.H., Walter, F.J., and Schmitt, H.W., Phys. Rev. 149, 894 (1966).

[34] Pleasonton, F.: Phys. Rev. 174, 1500 (1968).

[35] Brandt, R., Thompson, S.G., Gatti, R.C., and Phillips, L., Phys. Rev. 131, 2617 (1963).

[36] Pate, B.D., and Peter, J., Nucl. Phys. A173, 520 (1971).

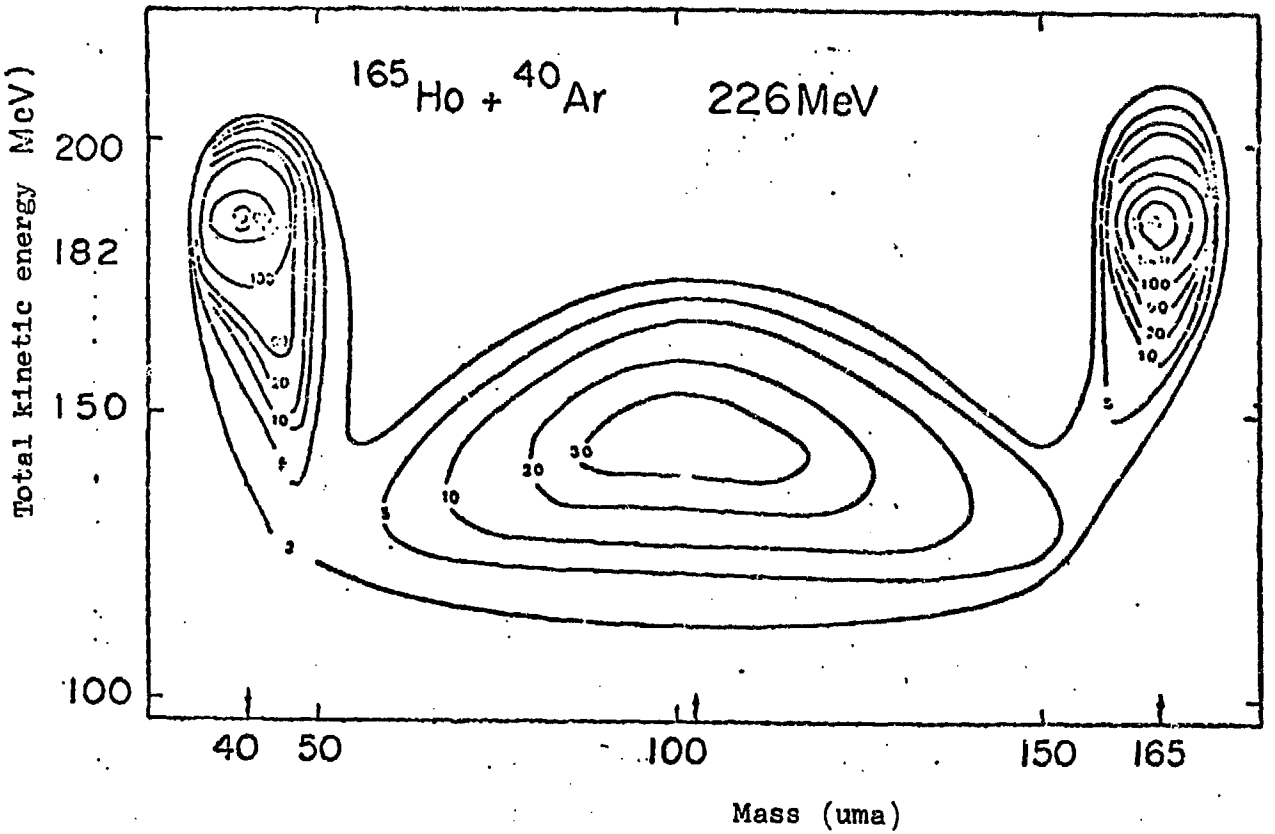

Fig. 1--226 MeV ^{40}Ar (182 MeV CMS) on ^{165}Ho target. Chart of total kinetic energy (CMS) x mass of product detected by detector X located at 59°. In addition to the binary fission fragments, a zone of scattered argons and tranfer products appears around 182 MeV x 40 uma, since the Rutherford maximum elastic scattering angle for the projectile is approximately 60°. There is also scattered Ho and transfer products around 226 MeV x 165 amu, since the Rutherford minimum scattering angle for the nucleus-target is about 54°.

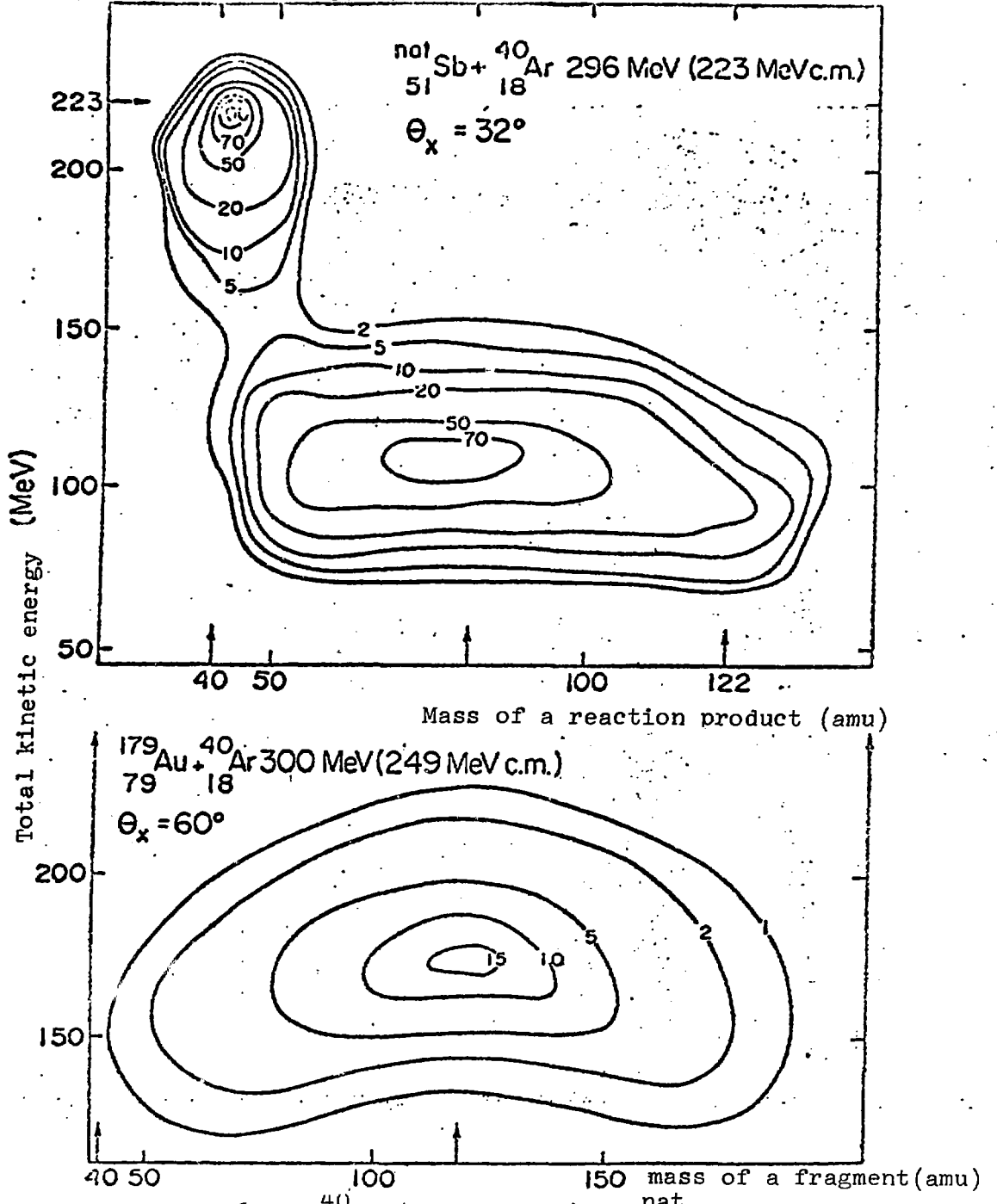

Fig. 2--Top: 296 MeV ^{40}Ar (223 MeV CMS) on ^{nat}SB target. Chart of total kinetic energy (CMS) x mass of product detected by detector X located at 32°. In addition to the binary fission fragments, scattered Ar and transfer products appear around 223 MeV x 40 amu, since the Rutherford maximum elastic scattering angle for the projectile is about 30°. There are no events at about 223 MeV x 122 since the Rutherford minimum scattering angle for the nucleus-target is about 70°. Bottom: 300 MeV ^{40}AR (249 MeV CMS) on ^{197}Au target. Detector X placed at 60° detects only fission fragments since the limit angles for Rutherford elastic scattering are 44° and 65° for the projectile and target, respectively.

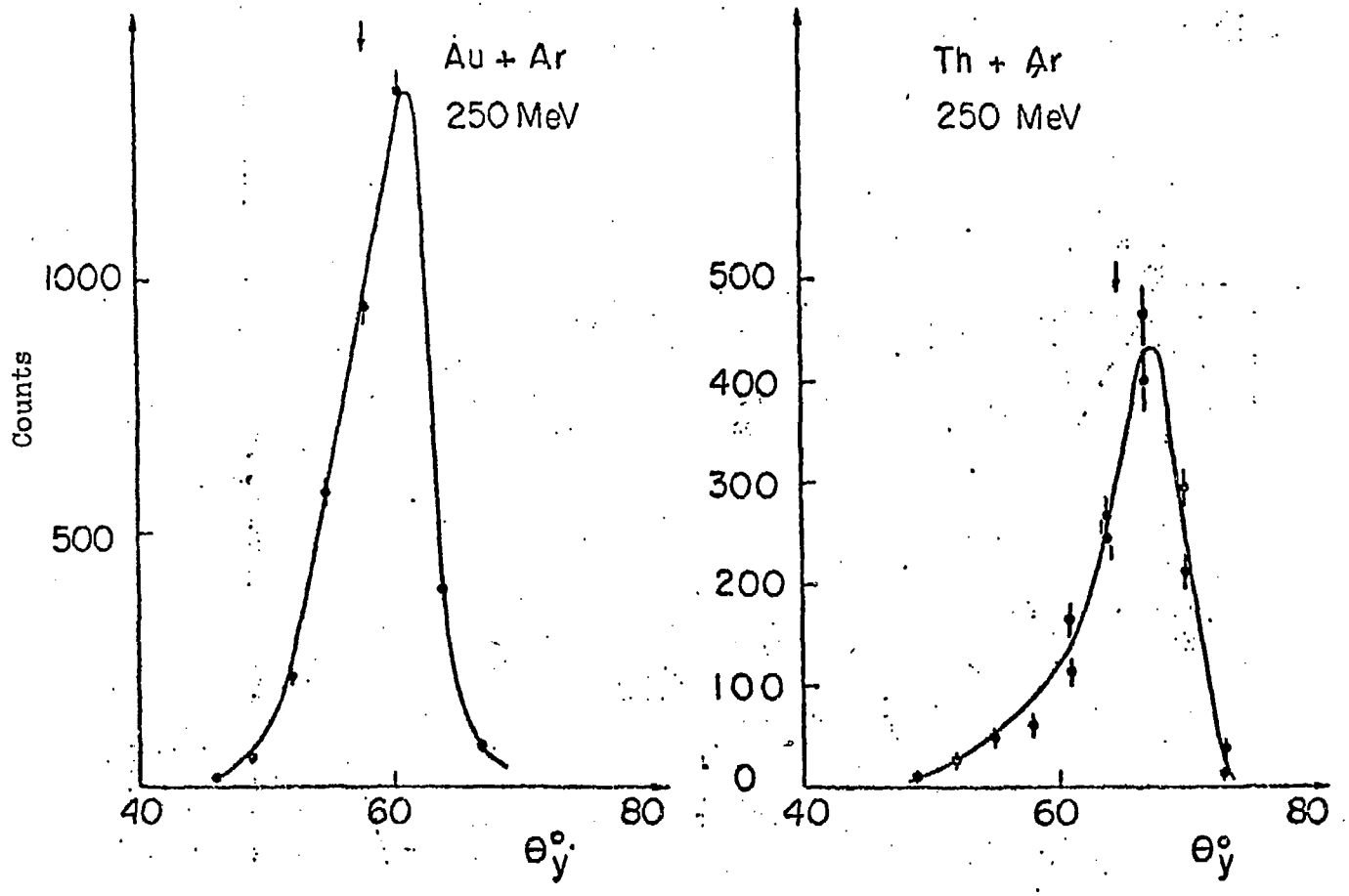

Fig. 3--Angular correlations between the fission fragments of ^{237}Bk and $^{272}108$ nuclei (Au and Th targets bombarded by 250 MeV Ar). The vertical arrow indicates the expected correlation for symmetrical fission according to the total kinetic energy predicted by Nix [3].

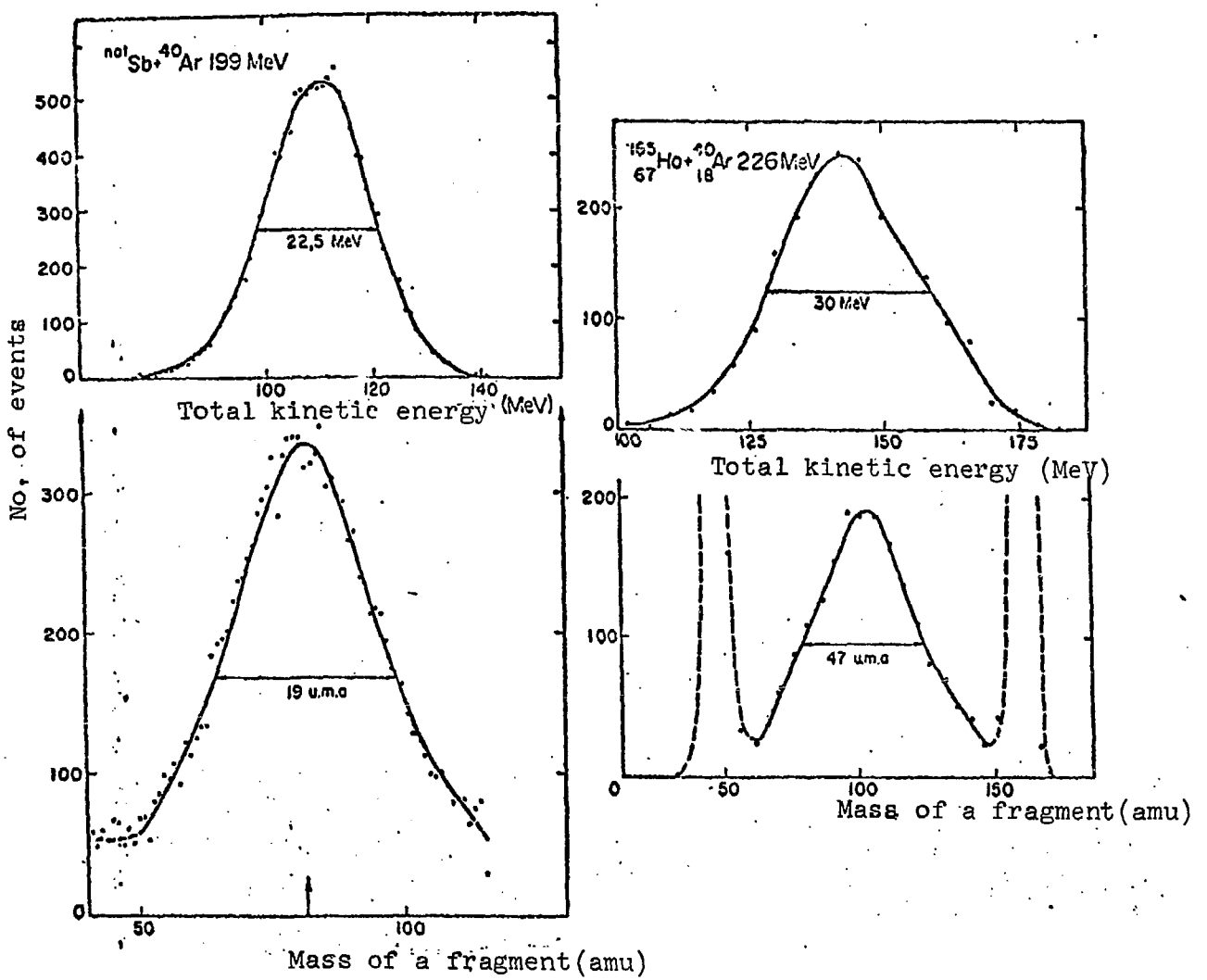

Fig. 4--Mass and total kinetic energy spectra for the fission fragments of ^{205}Ar nucleus excited to 97 MeV (^{165}Ho target, 226 MeV Ar ion) and of $^{161,163}Tm$ excited to 86 MeV (^{nat}Sb target, 199 MeV Ar ion).

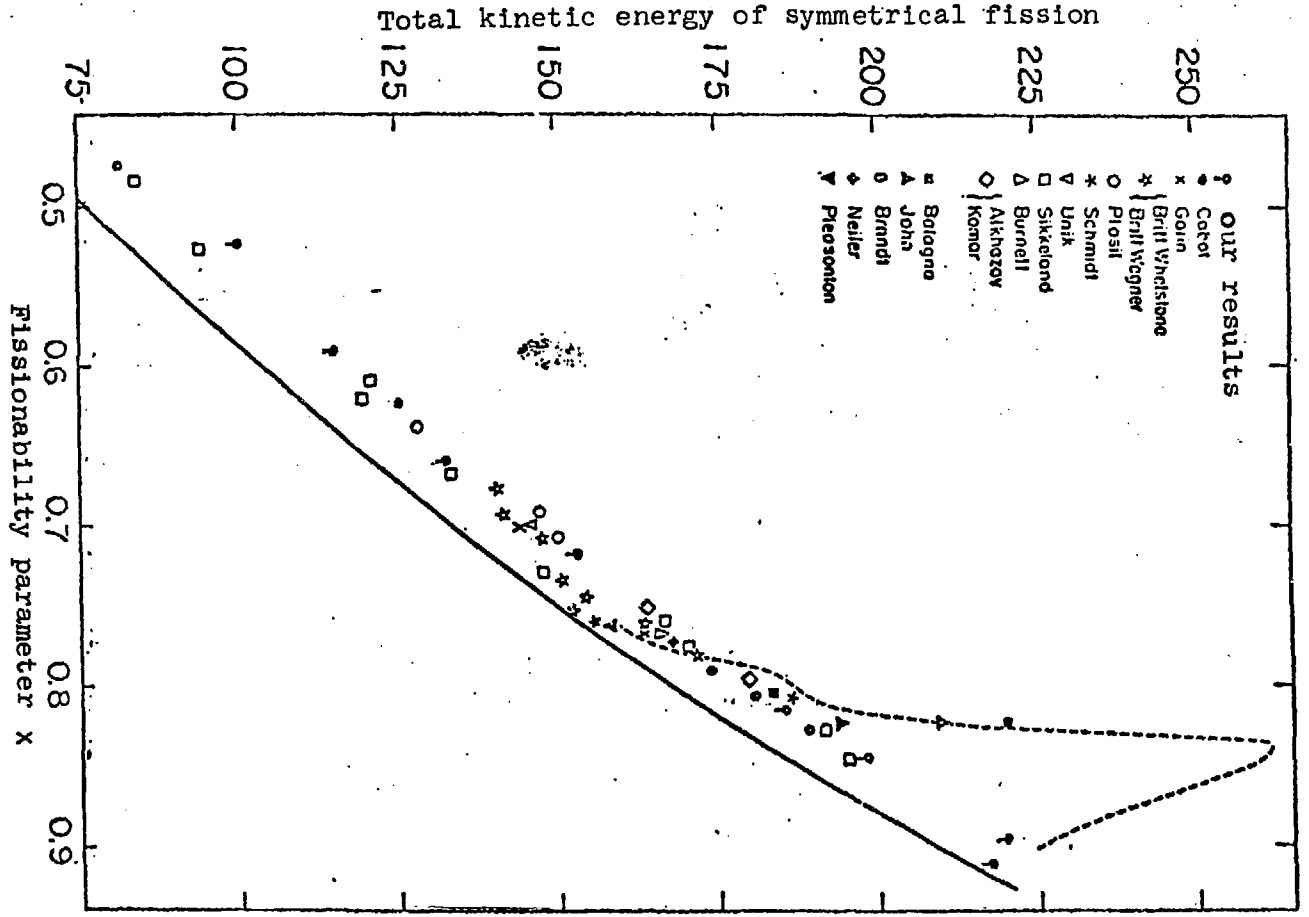

Fig. 5--Variation of the total kinetic energy for symmetrical fission (equal fragments) as a function of the fissionability parameter x. The continuous curve is the prediction of Nix [3]; the dashed curve is based on Schmitt and Mosel [12]. The different authors of the list correspond to references [20] to [35] in the order listed.

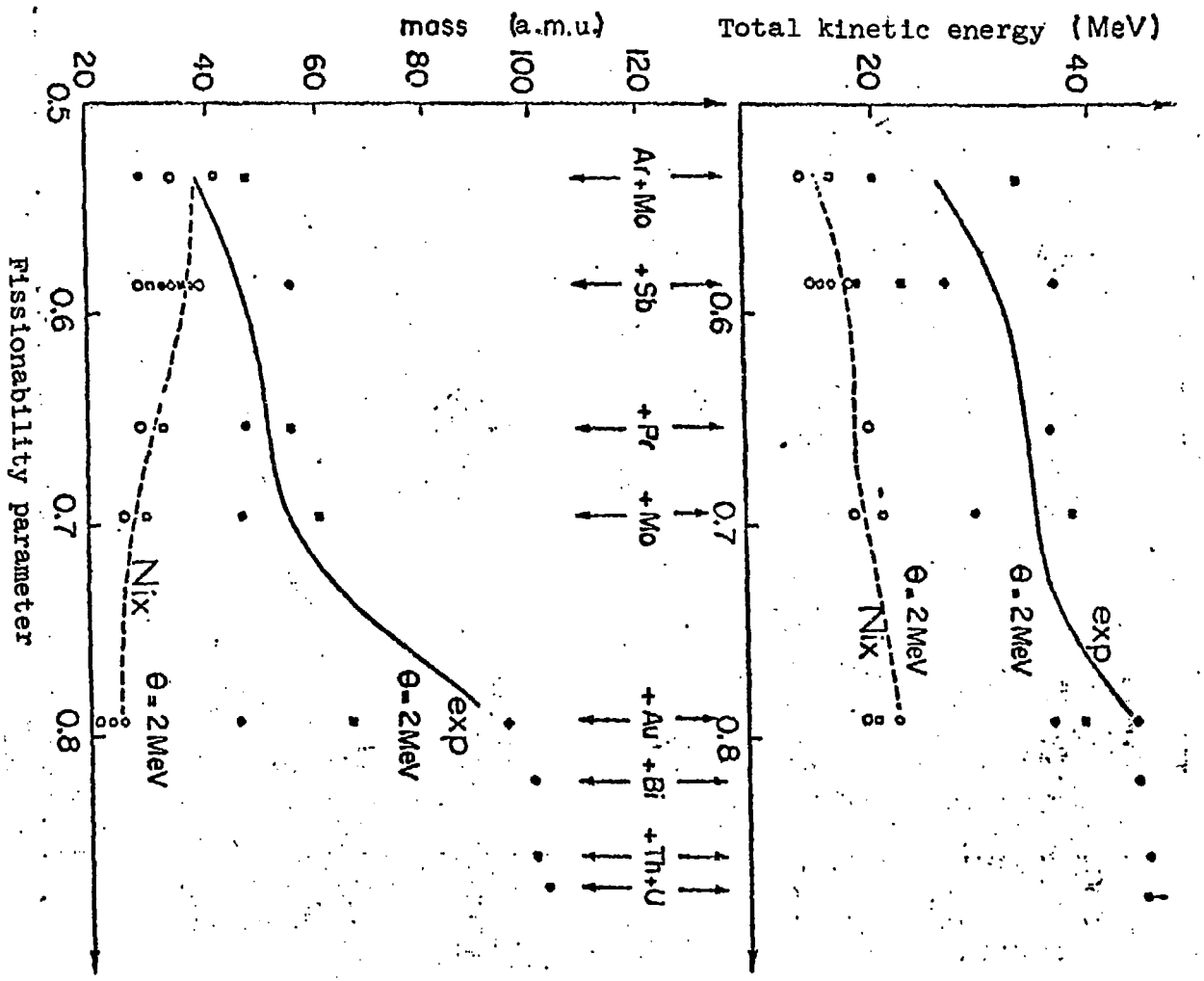

Fig. 6--Mass (bottom) and total kinetic energy distribution widths (top) for fission of different compound nuclei, as a function of the fissionability parameter x. The black symbols are the experimental results; the same open symbols are values calculated according to Nix [3] for the same value of x. The two curves show the variations with predicted and experimental x for the same nuclear temperature at the threshold.

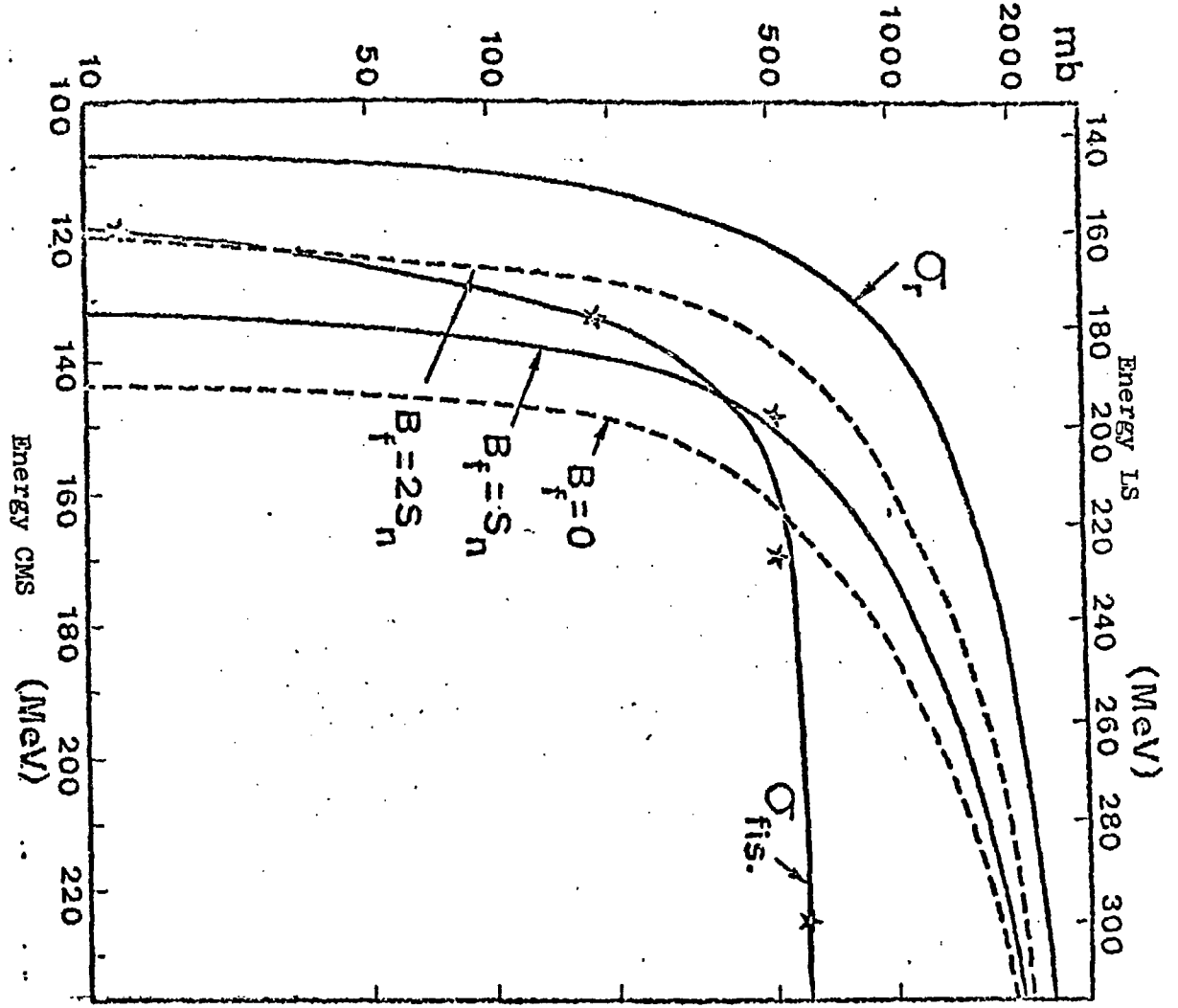

Fig. 7--Excitation function for fission of the fusion nucleus formed by Ar on a ^{nat}Sb target. The calculated curves correspond to different hypotheses for the angular momentum value where the nuclei fission begins (see text) and assume that there is no critical angular momentum for production of the fusion nucleus.

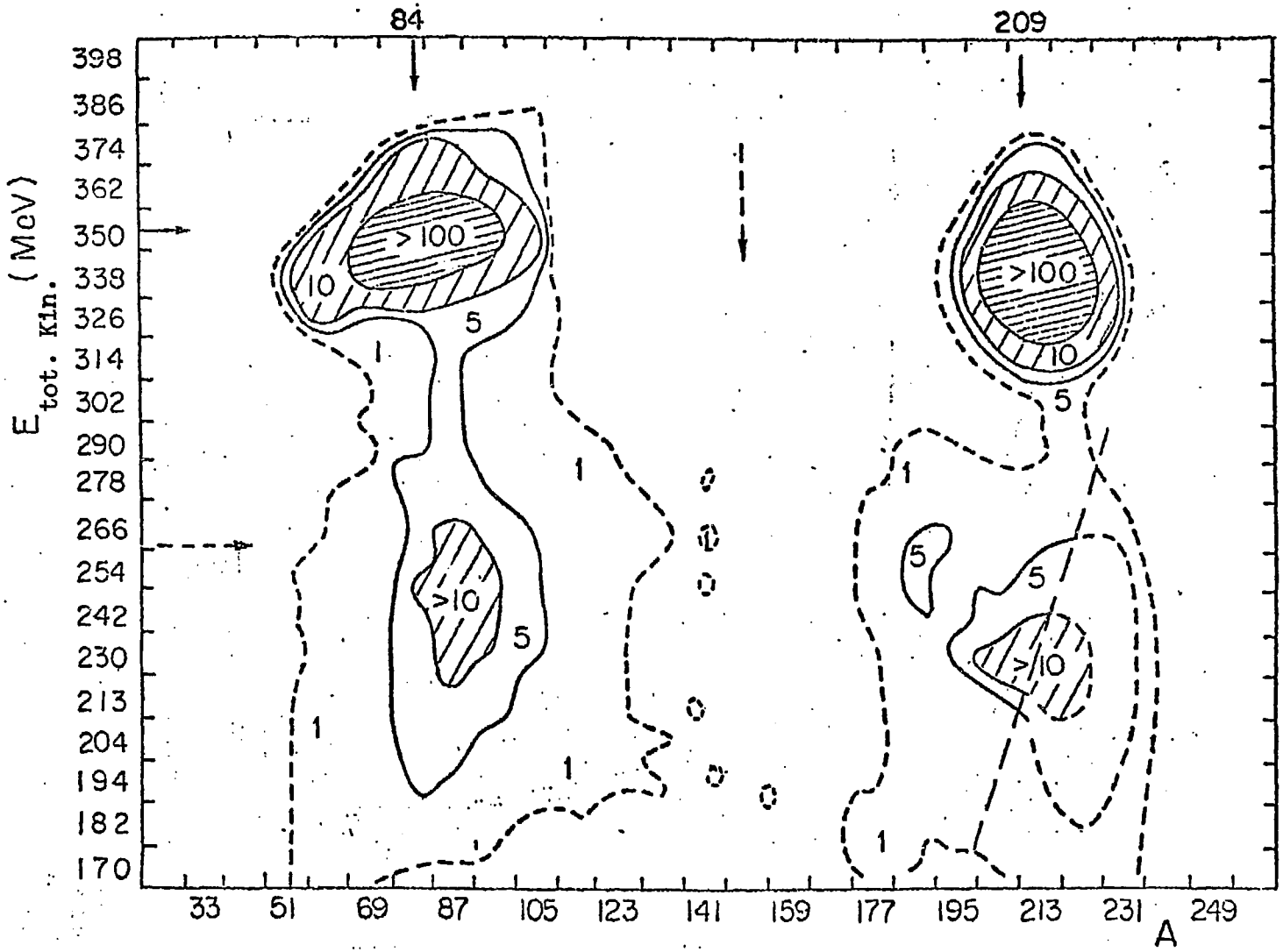

Fig. 8--500 MeV Kr (357 MeV CMS) on ^{209}Bi target. Chart of total kinetic energy CMS x mass of product detected by detector X located at 54°. Elastic scattering peaks (contour curves above 1000) and transfer products appear in the vicinity of A = 84 and 109, TKE = 357 MeV. The dashed arrows indicate the expected site of binary symmetrical fission events.